Biomass and Bioenergy 209 (2026) 109009

Contents lists available at ScienceDirect

Biomass and Bioenergy

journal homepage: www.elsevier.com/locate/biombioe

Assessing phase behavior of pyrolytic lignin in fast pyrolysis bio-oil via advanced distillation curve

Ana C.C. Araujo [a], Frederico G. Fonseca [b], Nicolaus Dahmen [a], Axel Funke [a,*]

[a] Institute of Catalysis Research and Technology (IKFT), Karlsruhe Institute of Technology (KIT), Hermann-von-Helmholtz Platz 1, 76344, Eggenstein-Leopoldshafen, Germany

[b] Institute for Low-Carbon Industrial Processes, German Aerospace Agency (DLR), 03046, Cottbus, Germany

ARTICLE INFO

Keywords:
Fast pyrolysis bio-oil
Pyrolytic lignin
Vapor-liquid equilibrium
Advanced distillation curve

ABSTRACT

Fast pyrolysis bio-oil (FPBO) holds promise as a renewable source for fuels and chemicals, yet its complex chemical composition poses significant challenges for efficient product recovery design and further downstream separation. In particular, the high molecular weight pyrolytic lignin fraction remains difficult to characterize, as its composition is largely unknown and its thermodynamic behavior poorly described. To improve understanding, the vapor-liquid equilibrium (VLE) behavior of FPBO was investigated, focusing on the pyrolytic lignin. A lignin-derived FPBO was selected for the study in order to minimize the influence of carbohydrate components of biomass. Advanced distillation curve (ADC) experiments were conducted to obtain thermodynamic data, which was then compared to simulations in which the FPBO was modeled as a surrogate mixture. To represent the pyrolytic lignin (PL) in the mixture, a range of surrogate molecules, from dimers to tetramers with varied inter-unit linkages and functional groups, were evaluated to find which structure best represents the PL in VLE calculations. Among the structures tested, dimers featuring biphenyl inter-unit linkages provided the best overall agreement to the experimental values. In general, dimers were more suitable for simulation, as some of the trimers and tetramers faced convergence issues and simulation errors. The effect of thermodynamic model was also taken into consideration, comparing the Ideal equilibrium model, the UNIFAC-Dortmund (DMD) activity coefficient method, and the Peng-Robinson Boston-Mathias (PR-BM) equation of state. The findings underscore the importance of surrogate and model selection and provide guidance for optimizing FPBO fractionation and upgrading.

1. Introduction

Fast pyrolysis has emerged as a promising technology for the valorization of lignocellulosic biomass, offering a renewable pathway for producing fuels and chemicals [1]. This thermochemical process rapidly converts the major components of biomass – cellulose, hemicellulose, and lignin – into a liquid product known as fast pyrolysis bio-oil (FPBO), alongside smaller amounts of gases and char [2]. FPBO is particularly attractive due to its high liquid yield and ease of storage and transport; however, it is a chemically complex emulsion, comprising water, light oxygenated compounds (e.g., acids, alcohols, and ketones), monomeric phenols, sugars, and lignin-derived oligomers [3]. While many of these components hold significant promise for industrial applications, such as resins, coatings, and biofuels, others, such as water and highly oxygenated species, contribute to FPBO's corrosiveness, low heating value, and chemical instability, limiting its direct use [4].

To improve FPBO's properties and broaden its applicability, different fractionation and upgrading techniques have been explored to reduce oxygen content, enhance stability, and increase its calorific value, as well as isolate valuable compounds for potential commercialization [5,6]. Fractional condensation is a commonly employed strategy, separating pyrolysis vapors into distinct fractions based on their dew points [7]. This approach allows for the selective recovery of lighter, more reactive components and heavier fractions enriched in phenolics [8,9]. Liquid-liquid extraction offers another method for isolating specific chemical groups, enabling the removal of sugars or phenols for targeted applications [10,11]. Despite these advancements, designing and optimizing these processes requires a deep understanding of FPBO's behavior in phase equilibria at varying conditions. Modeling FPBO processes is a powerful tool for simulating, optimizing, and predicting

* Corresponding author.
E-mail address: axel.funke@kit.edu (A. Funke).

https://doi.org/10.1016/j.biombioe.2026.109009
Received 26 September 2025; Received in revised form 16 January 2026; Accepted 20 January 2026
Available online 28 January 2026

the performance of bio-oil production systems [12]. However, achieving accurate and reliable models for FPBO remains a significant challenge due to the highly complex and variable nature of its composition [13].

A particularly challenging component within FPBO is the pyrolytic lignin (PL), a high molecular weight fraction primarily derived from the thermochemical breakdown of lignin during pyrolysis. The PL is composed of oligomers with aromatic structures and a wide range of molecular weights [14,15]. Its content in FPBO can vary substantially, typically accounting for 15–50 wt% of the total bio-oil, depending on both the feedstock and the specific process conditions [16–18]. The presence of PL has a pronounced impact on the physicochemical properties of FPBO, including viscosity, phase stability, solubility, and reactivity [19,20]. These properties, in turn, affect downstream processing steps such as upgrading, separation, and utilization in fuel or chemical applications. It has been previously shown that the representation of this fraction is particularly important for improving the predictive capability of phase equilibrium models [21,22]. In addition, high molecular weight compounds derived from carbohydrates may also be present in FPBO, which further increases the complexity of modeling effects [23,24].

The complexity of the PL poses several modeling challenges. First, its chemical structure is not uniform; it consists of a broad distribution of oligomeric species with varying degrees of polymerization, functional group content, and solubility [17,20]. This makes it difficult to represent PL as a single component or even as a well-defined group of compounds during process simulation [13,22,25]. Second, the interactions between PL and other bio-oil constituents can lead to phase separation and unpredictable changes in physical properties, complicating both experimental characterization and predictive modeling [19,21].

Advanced modeling approaches for this PL fraction often incorporate surrogate compounds, pseudo-components, or group contribution methods to describe the behavior of pyrolytic lignin. Recent research has also focused on integrating experimental data such as molecular weight distributions, functional group analyses, and phase behavior studies, into modeling frameworks to improve their predictive power [22,25–27]. However, selecting appropriate surrogates is still challenging, as the absence of direct experimental data on key thermophysical properties introduces uncertainties in phase equilibrium modeling [13,26].

The advanced distillation curve (ADC) method provides a robust tool for investigating the VLE behavior of FPBO and acquiring detailed thermodynamic data [28]. In contrast to conventional distillation techniques, ADC generates a comprehensive dataset by recording temperature, pressure, and composition at discrete distilled volume fractions throughout the distillation process, offering valuable insights into the phase behavior of complex bio-oils [29]. This method is well-suited for thermally sensitive systems, as it can operate under reduced pressure to mitigate undesirable phenomena such as polymerization and thermal degradation [30]. The thermodynamic data obtained from ADC experiments constitutes a valuable resource for refining thermodynamic models, optimizing surrogate mixtures, and enhancing the predictive accuracy of VLE models for FPBO [31].

In this study, the representation of pyrolytic lignin in FPBO models was investigated to find the most suitable approach for improving VLE predictions. To achieve this, ADC experiments were integrated with VLE simulations to obtain a comprehensive understanding of FPBO's phase behavior, with a particular emphasis on the influence of pyrolytic lignin. To isolate and elucidate the thermodynamic role of the pyrolytic lignin, FPBO derived specifically from lignin was selected, allowing for a focused assessment of this high molecular weight fraction without the interference of carbohydrate derived compounds. The ADC experiments yield detailed temperature and composition profiles for each distilled fraction of FPBO, which were subsequently modeled using the IDEAL model, the UNIFAC-Dortmund (DMD) activity coefficient model, and the Peng–Robinson Boston–Mathias (PR-BM) equation of state, using different surrogate molecules to represent the pyrolytic lignin fraction. The insights gained from this combined experimental and modeling approach advance the understanding of the thermophysical properties of FPBO and provide a foundation for more accurate and efficient models for bio-oil processing and upgrading.

2. Materials and methods

2.1. Lignin fast pyrolysis bio-oil

The lignin bio-oil used in this study was produced via fast pyrolysis of a *Miscanthus* derived lignin (Miscancell), as detailed in a previous work [32]. In the study, pyrolysis experiments were conducted at 500 °C in an auger type reactor that mechanically mixes the feedstock with a preheated heat carrier (steel beads) with a feedstock capacity of 10 kg/h. Residence time of the solids in the reactor are 10–15 s; the gas residence time is estimated to be < 2 s [33]. Entrained char particles are separated from hot pyrolysis gases in a series of two cyclones and a ceramic filter prior to condensation in a tube and shell condenser integrated in an electrostatic precipitator that operates at 90 °C. The condensate collected at this temperature was used as bio-oil in this study and characterized for its elemental composition, density, water content (via Karl Fischer titration) and chemical composition (via GC-MS/FID). Key results are summarized in Table 1.

2.2. Advanced distillation curve experiments

Vacuum advanced distillation curve experiments using the lignin bio-oil were conducted following the approach reported by Krutof and Hawboldt [28], a scheme of the setup can be found in Fig. 1. At the beginning of each experiment, the system was evacuated to an absolute pressure of 15 kPa, after which heating was initiated. The sample was placed in a round-bottom flask enclosed by a heating jacket programmed to follow a three-stage heating ramp from room temperature to 285 °C. Vapor condensation was achieved using a counter-flow condenser initially cooled to 0 °C.

The first measurement was recorded when the first droplet of condensate was visually observed. Subsequently, kettle and head temperature were recorded at every 10 mL interval, as observed on the calibrated receiving flask. At the same points, 10 μL samples were taken using a syringe for GC-FID analysis. Distillation continued until no further condensation was observed. All experiments were carried out in triplicate to ensure reproducibility.

A few adaptations were made to the setup described by Krutof and Hawboldt [28]. To accommodate for a smaller sample size used in the study (100 mL vs, 200 mL), a 250 mL round-bottom flask was used

Table 1
Properties of the lignin FPBO used in the study (adapted from Ref. [32]).

Property	Lignin FPBO
General properties	
Water content (wt.%)	12.5
Density at 60 °C	1.11
Elemental composition (wt.%)	
C	60.4
H	6.1
O	30.7
Chemical composition (wt.%)	
Acids	8.2
Ketones	1.2
Furans	0.4
Benzenes	0.6
Phenols	3.9
Guaiacols	6.1
Syringols	3.6
Sugars	2.1

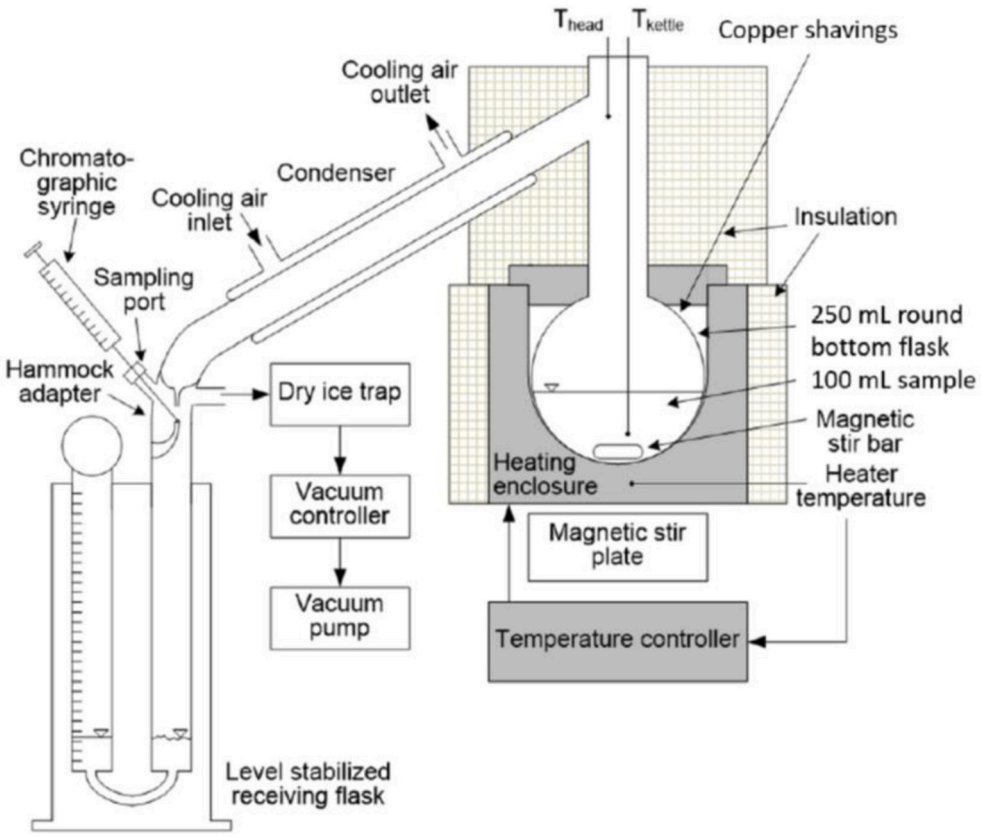

Fig. 1. Scheme of vacuum ADC system adapted from Ref. [28].

instead of a 500 mL one, and the gap between the flask and the heating enclosure was filled with copper shavings to improve heat transfer. In addition, the lower pressure of 5 kPa used in the original work could not be achieved due to equipment limitations.

2.3. Modeling

Modeling of the ADC experiments was carried out using Aspen Plus V14®. The thermodynamic property method used was either IDEAL, UNIFAC-DMD, or PR-BM for comparison purposes; property methods were not modified from their default configurations [34]. All molecules were characterized based on their structure, and in the case of the UNIFAC-DMD model, functional group information was also required. Properties that were not present in the Aspen Properties™ database were estimated using default options. Details can be found in the Supplementary Information (SI).

For the bio-oil properties, the elemental composition was determined by performing a simple component balance over the surrogate mixtures, using the different PL surrogate molecules. Density predictions were obtained by simulating the bio-oil surrogate mixtures in Aspen at 60 °C, matching the reference temperature of the experimental data.

For the VLE calculations, a scheme of the flowsheet model can be found in Fig. 2. The process was simulated at an absolute pressure of 15 kPa, with the lignin FPBO input as a liquid at 25 °C and a flow rate of 100 L/h. Each distillation stage was modeled as a *HEATER* + *SEP2* pair, with the *HEATER* configured to achieve a specified vapor fraction and the *SEP2* unit serving as an adiabatic separator. Design specifications were applied at each stage to evaporate 10 L of the liquid input by adjusting the vapor fraction in the *HEATER*, corresponding to the volume intervals of the ADC experiments. For the very first drop, however, no design specification was applied, and a fixed vapor fraction of 1×10^{-6} was used instead. The vapor stream produced in each stage was condensed using a second *HEATER*, enabling evaluation of the recovered condensate fractions. This approach allowed for the prediction of the temperature profile along the distillation and the component distribution across the collected fractions.

The lignin FPBO was modeled using a surrogate mixture, as detailed in Table 2. The selected components and their weight fractions were based on data from the previous bio-oil GC-MS/FID characterization summarized in Table 1; the remaining unidentified fraction was represented as pyrolytic lignin.

The pyrolytic lignin (PL) surrogate was modeled using various molecules proposed in the literature to evaluate which structure best represents the bio-oil properties and VLE behavior. A similar set of structures were also employed by Rojas et al. [22] when modeling liquid-liquid equilibrium. The molecules were grouped according to shared structural characteristics, such as number of aromatic rings and linkage type, as summarized in Table 3. To illustrate these differences, Fig. 3 shows a representative molecule from each group, highlighting the base structure and typical size. Full information on the structure, molecular formula, and functional groups of all molecules is provided in the SI. From this point on, these molecules will be referred to as PL surrogates. In modeling, all molecules were evaluated individually, meaning no mixture of PL surrogates was considered. Additionally, a surrogate mixture excluding the PL surrogate, referred to as "No-PL," was evaluated to assess the importance of including pyrolytic lignin in the overall representation. This No-PL mixture contained only the components identified during the characterization, with their weight fractions normalized to 100 %.

2.4. Data treatment

All simulated property values were processed and analyzed against the experimental data. Experimental reference values for elemental composition and density were taken from the characterization of the lignin FPBO reported on Table 1. For VLE evaluation, the experimental

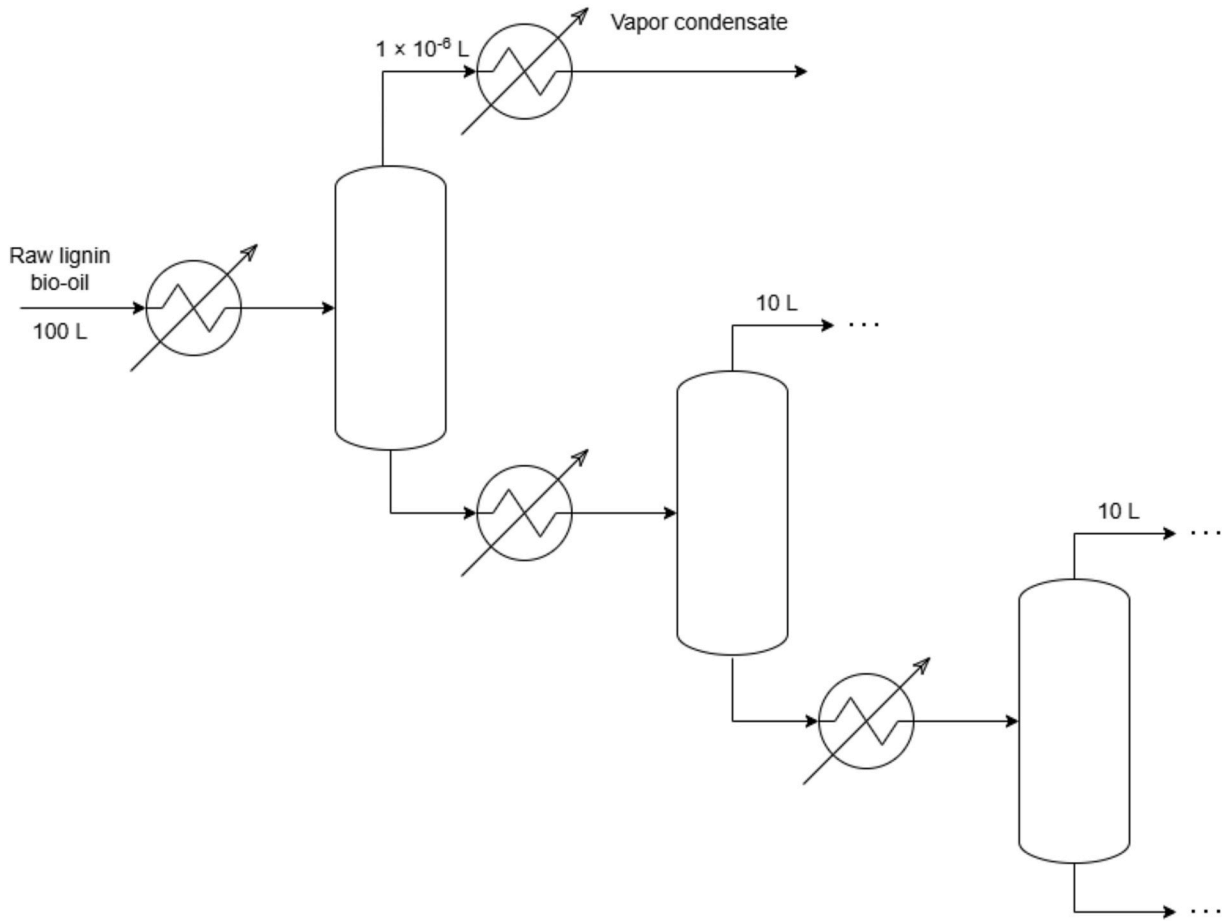

Fig. 2. Scheme of the model implemented in Aspen Plus™, based on the flowsheet view of the software environment.

Table 2
Surrogate mixture of the lignin FPBO.

Component	Mass Fraction	Formula	CAS
Acetic Acid	3.31 %	$C_2H_4O_2$	64-19-7
Propionic acid	4.97 %	$C_3H_6O_2$	79-09-4
Cyclopentenone	0.56 %	C_5H_6O	930-30-3
Cyclopentenone, 2-methyl	1.32 %	C_6H_8O	1120-73-6
2(H)-Furanone	0.42 %	$C_5H_4O_2$	98-01-1
Benzofuran	0.59 %	C_8H_6O	271-89-6
Phenol	1.32 %	C_6H_6O	108-95-2
P-cresol	1.32 %	C_7H_8O	106-44-5
Phenol, 4-ethyl	1.32 %	$C_8H_{10}O$	123-07-9
Guaiacol	1.84 %	$C_7H_8O_2$	90-05-1
Guaiacol, 4-vinyl	1.23 %	$C_9H_{10}O_2$	7786-61-0
Isoeugenol	1.84 %	$C_{10}H_{11}O_2$	5932-68-3
Acetoguaiacone	1.23 %	$C_9H_{10}O_3$	498-02-2
Syringol	1.64 %	$C_8H_{10}O_3$	91-10-1
Syringol, 4-vinyl	1.64 %	$C_{10}H_{12}O_3$	28343-22-8
Acetosyringone	0.37 %	$C_{10}H_{12}O_4$	2478-38-8
Levoglucosan	2.11 %	$C_6H_{10}O_5$	498-07-7
Water	12.25 %	H_2O	7732-18-5
Pyrolytic Lignin Surrogate	60.93 %	–	–

data of the ADC temperature profile and water content across the distillation range were used.

The relative error (RE) was used for properties with a single experimental value, such as density:

$$RE = \left| \frac{x_{sim} - x_{exp}}{x_{exp}} \right| \times 100 \quad (1)$$

For properties with multiple data points, such as elemental composition and ADC profiles, the mean absolute relative error (MARE) was used:

$$MARE = \frac{1}{n} \sum_{i=1}^{n} \left| \frac{x_{sim,i} - x_{exp,i}}{x_{exp,i}} \right| \times 100 \quad (2)$$

In addition, for evaluating the different groups of molecules, the mean MARE of each group's molecules was used, following the grouping logic defined in Table 3.

Table 3
Classification of PL surrogates by structure and linkage type, following the group approach from Ref. [22].

Group	Description	Molecules	Reference
D-A	Dimer – β-O-4	D-A1, D-A2, D-A3, D-A4	[26,35]
D-B	Dimer – Biphenyl	D-B1, D-B2, D-B3, D-B4	[21,36]
D-C	Dimer – Stilbene	D-C1, D-C2	[36,37]
D-D	Dimer – Phenylcoumaran	D-D1, D-D2	[36]
D-E	Dimer – Resinol	D-E1	[36]
D-F	Dimer – Bridging double bond	D-F1	[38]
TR	Trimer – various links	TR1, TR2, TR3, TR4, TR5, TR6	[26,37,39]
TE	Tetramer – various links	TE1, TE2	[37,40]

3. Results and discussion

3.1. ADC experiments

The kettle temperature results obtained from the ADC experiments of

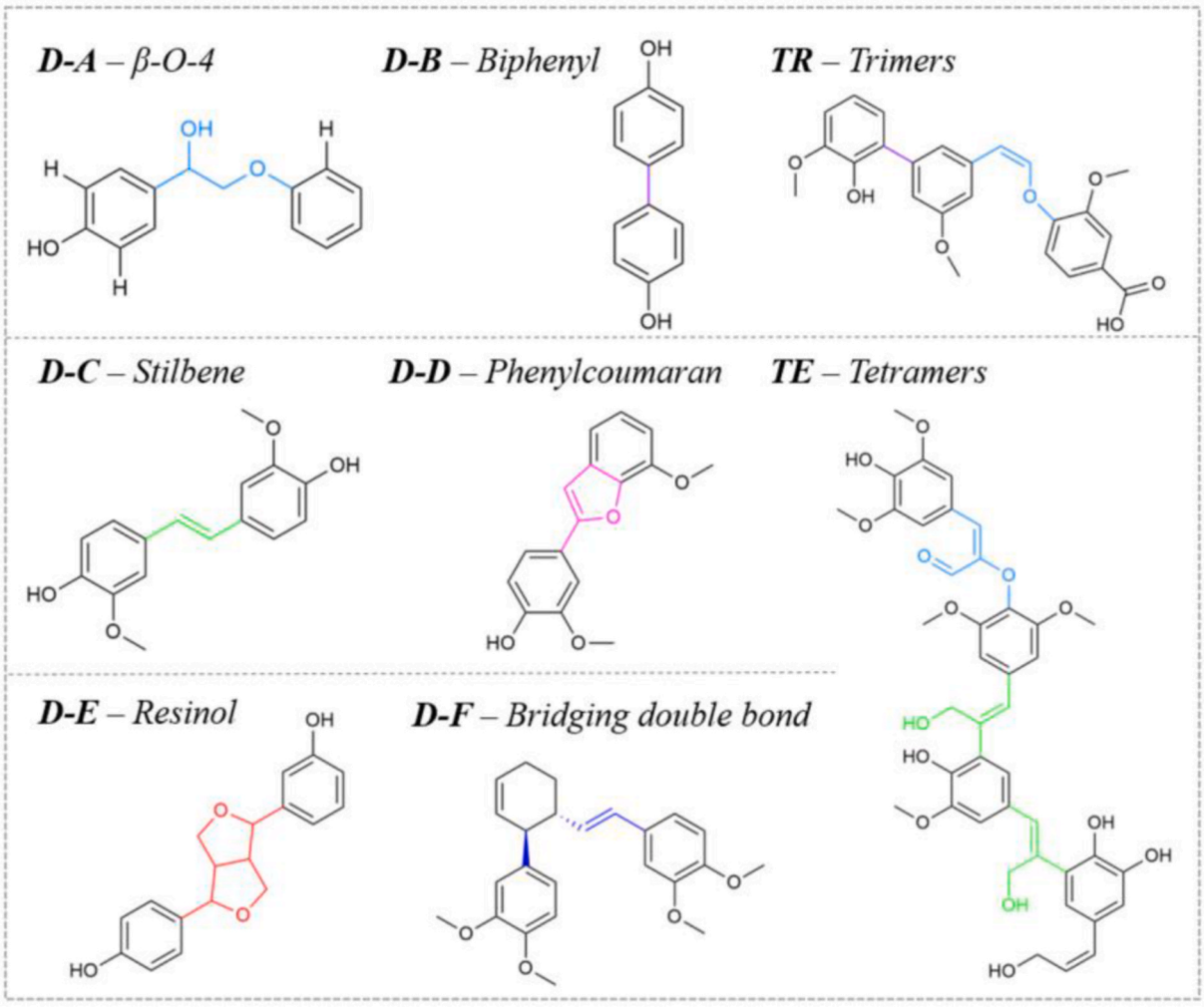

Fig. 3. Representative PL surrogate from each group.

the lignin FPBO can be seen in Table 4. At the distillation starting point (57.6 °C), temperature values were consistent across replicates, with a standard deviation of 0.5 °C. Following this, the temperature increased to an average of 96.9 °C at 10 % distilled volume. An even sharper increase was observed at 20 %, with temperature reaching 189.1 °C. This point also exhibited the highest deviation across replicates (22.6 °C), indicating a broader range of volatiles present in this fraction. From that point on, temperature gains became less pronounced, stabilizing toward the final measured values and showing lower deviations.

The temperature results presented in Table 4 are compared with the data reported by Krutof and Hawboldt [28], for a softwood bio-oil, in Fig. 4. Given the limited availability of ADC data for bio-oils, particularly lignin-derived ones, the softwood bio-oil results are used here as a comparative reference. Comparing the curves, the two distillation profiles show significant differences. Krutof and Hawboldt [28] reported an earlier distillation onset (33.4 °C) and a convex profile with a lower incline. In contrast, this work presents a sharper incline and a more concave profile, with distillation starting at higher temperatures. Furthermore, the distillation of softwood bio-oil proceeds up to ~65 vol % distilled, whereas in this work it was limited to ~40 vol% Interestingly, despite these differences, both curves reach similar final temperatures near 260 °C.

Table 4
Kettle temperatures from ADC of lignin fast pyrolysis bio-oil at 15 kPa.

Distilled volume %	Experimental kettle temperature (T_{kettle}, °C)				
	Run 1	Run 2	Run 3	Average	St. deviation
0	56.9	57.9	58	57.6	0.5
10	93.9	81.3	115.5	96.9	14.1
20	162.9	186.4	218	189.1	22.6
30	219	227	247	231	11.8
40	244	251	262	252.3	7.4

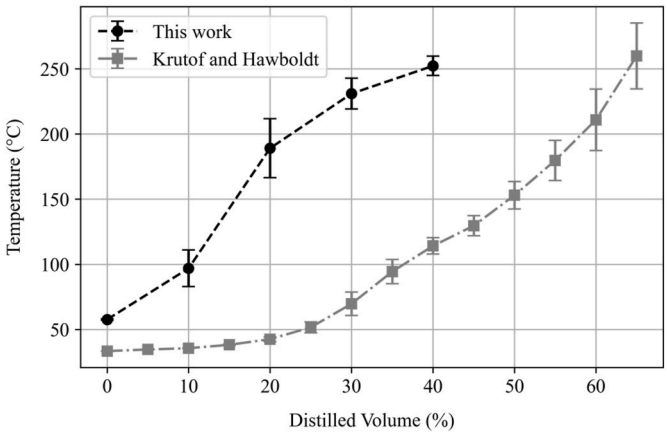

Fig. 4. ADC temperature profiles of lignin FPBO at 15 kPa (this work) and softwood fast pyrolysis bio-oil at 5 kPa (Krutof and Hawboldt [28]).

These variations can be attributed to both the distinct nature of the bio-oils and the experimental conditions. The lignin-derived bio-oil used here contains a higher proportion of heavy phenolic oligomers and pyrolytic lignin, whereas softwood-derived oil likely includes more water and light volatiles. Additionally, the lower vacuum pressure employed by the reference (5 kPa vs 15 kPa in this study) would favor earlier and more extended evaporation of volatile fractions, further amplifying the observed differences.

In addition to the temperature data, the ADC experiment also provides insight into the distribution of compounds across the distilled fractions, as shown in Fig. 5. Fig. 5a shows how the water content varies throughout the distillation, starting as the dominant component at approximately 80 wt% of the initial fraction and gradually decreasing as the distillation progresses. It is interesting to note that at 15 kPa, the boiling point of pure water is approximately 54.8 °C [41], closely aligning with the initial temperature observed in our experiments (57.6 °C). The slight elevation could be attributed to the presence of other solutes in the mixture. In contrast, at 5 kPa, water boils at around 32.9 °C [41], which corresponds well with the distillation onset reported by Krutof and Hawboldt (33.4 °C). This supports the conclusion that the difference in starting temperatures between the two curves shown in Fig. 4 is primarily due to the difference in operating pressure.

To further assess the phase behavior of water, its experimental activity coefficient (γ) in the initial distillation stage was estimated via modified Raoult's law. Based on the water content measured in the condensate at the starting point and the composition of the liquid surrogate mixture (Table 2), the mole fractions of water in each phase were determined. Two scenarios were considered to account for the uncertainty in the composition of the pyrolytic lignin (PL) surrogate: one assuming the smallest PL molecule in the surrogate set (D-B1) and another the largest (TE2). Calculations estimated activity coefficients of 1.76 and 1.42, respectively, which indicates a moderate positive deviation from ideal behavior, consistent with previous findings by Ille et al. [21]. Full calculation details are provided in the SI. Notably, the higher γ value was obtained for the smaller PL surrogate, which can be attributed to mole fraction balance, in which smaller molecules contribute a greater number of moles to the mixture, thereby lowering the mole fraction of water and increasing the calculated activity coefficient.

Fig. 5b presents the mass fraction of compounds identified by GC–FID and the remaining "unknown" fraction, calculated by subtracting the identified species and water content from the total. In the initial fractions, only a small portion of the distillate could be identified, and a notable fraction remained classified as unknown. The presence of these unidentified components at such early stages is somewhat unexpected and may arise from limitations in the GC–FID analysis and/or an underestimation of the water content. At 20 % distilled volume, both identified and unknown fractions reached amounts around 30 wt% and exhibited the highest standard deviations. This correlates with the peak deviations in temperature and water content, indicating an increased complexity in this fraction. In the final stages of the distillation (30–40 % distilled volume), the amount of identified compounds gradually declined, and with water content at its lowest, the unknown fraction became increasingly dominant, probably composed of pyrolytic lignin oligomers that are beyond the detection range of the GC–FID.

3.2. Modeling of FPBO properties

To evaluate how well different PL surrogate molecules represent the bulk characteristics of the lignin-derived FPBO, key physicochemical properties were analyzed. Fig. 6 presents a Van Krevelen diagram (H/C vs. O/C) for the surrogate mixtures using different PL molecules, alongside the experimental value for the lignin bio-oil. Each point represents one surrogate, with the color scale indicating the MARE in elemental composition compared to the experimental result. Full results for each individual molecule can be found in the SI.

From the graph, it is clear that the introduction of a PL surrogate significantly improves the representation of the lignin bio-oil's elemental composition, with the No-PL case showing the largest error (45 %), twice the error of worst performing surrogate. The best-performing PL surrogate, D-B1, is a small biphenyl-type dimer with just two oxygen atoms, yielding a MARE of 4.5 %. In contrast, TR5, a bulky trimer containing 15 oxygen atoms, produced the highest error at 24.8 %. These results indicate that PL surrogates with lower oxygen and higher carbon content more effectively capture the elemental composition of pyrolytic lignin. This suggests that the actual PL structures present in the heavy fraction of the bio-oil may be less oxygenated than those often assumed in the literature.

Accurately predicting the density of the bio-oil is essential as it reflects how well the surrogates capture bulk physical properties. Fig. 7

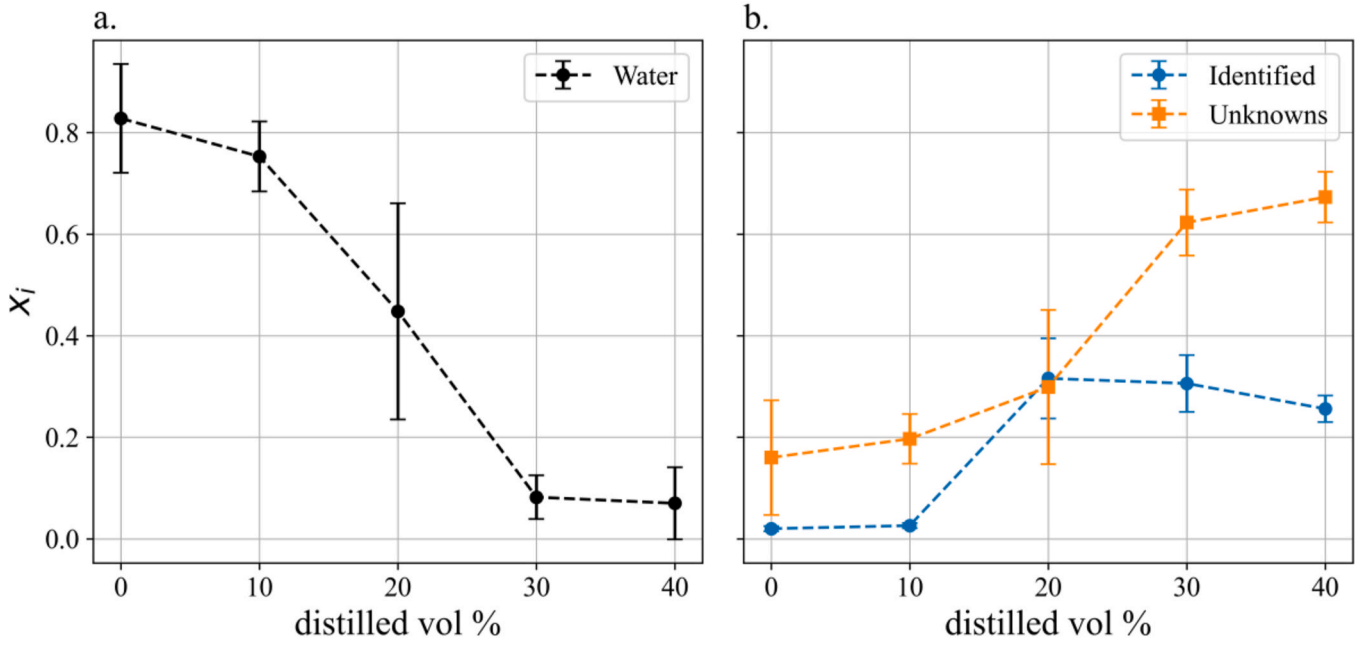

Fig. 5. Mass fractions of water (a), and GC–MS/FID identified vs. unknown compounds (b) in the ADC distillates.

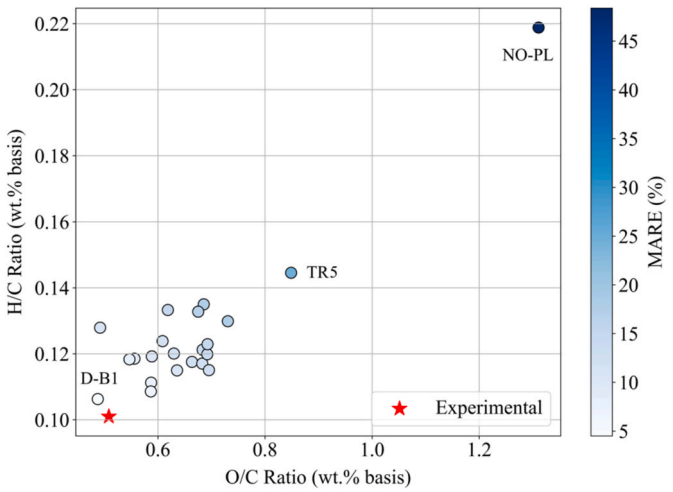

Fig. 6. Van Krevelen diagram (H/C vs. O/C) of bio-oil composition predicted by the different surrogate molecules. Color scale shows the error (MARE) in reproducing the experimental values. Representative molecular structures are provided in Fig. 3. (For interpretation of the references to color in this figure legend, the reader is referred to the Web version of this article.)

compares simulated density values (ρ) for surrogate molecules as a function of their molecular weight (MW) using two different methods: the Rackett equation, which is used by the IDEAL and UNIFAC-DMD models to estimate the liquid density, and PR-BM, which determines it from its own equation of state [34]. Full results are available in the SI. For the Rackett estimations (Fig. 7a), the best agreement was observed for dimers, particularly those in the 200–350 g/mol range, with most values falling close to the experimental target. As molecular weight increased, the predicted density generally declined, with most trimers and tetramers significantly underestimating the density, with the exception of TE1, which over predicted but still showed a considerably lower error.

In contrast, the PR-BM method (Fig. 7b) systematically predicted lower density values across all surrogates, showing larger deviations from the experimental target. While dimers still performed comparatively better than larger molecules, their predicted densities were generally lower than those obtained using the Rackett method. The discrepancy became more pronounced for trimers and tetramers, which showed limited predictive reliability, with many of these molecules encountering simulation issues and yielding zero-value predictions that were no included in the graph. These findings reinforce the limitations of cubic equations of state in representing liquid densities of heavy aromatics, as noted in previous studies [13].

The No-PL case underestimated the experimental density with both methods (Fig. 7), with the Rackett method performing better than PR-BM, which showed a larger underestimation. This shows that including a PL surrogate can improve predictive accuracy; however, this improvement depends strongly on the surrogate choice, as higher molecular weight candidates can often underestimate the density or lead to simulation issues.

The combined analysis of elemental composition and density showed that dimers yielded more reliable predictions, whereas high molecular weight surrogates, particularly those rich in oxygen, were less accurate and more prone to simulation errors. The D-B group (biphenyl-type dimer) consistently showed the best performance as surrogate for the pyrolytic lignin fraction, with other surrogates from the D-A (β-O-4), D-C (stilbene), and D-D (phenylcoumaran) groups also yielding strong results. These findings suggest that small, condensed aromatic dimers with low oxygen content are particularly well-suited to represent the physical properties of pyrolytic lignin in thermodynamic modelling.

3.3. Modeling of vapor-liquid equilibrium

To evaluate the ability of PL surrogates to reproduce VLE behavior, their performance was assessed using the experimental ADC data as benchmark. At first, the surrogates were evaluated by group, using the mean MARE for each group, with error bars indicating the standard deviation within the group. Some surrogates encountered simulation issues: TE2 failed to converge with the UNIFAC-DMD model and, while it ran with the IDEAL model, produced unrealistic results and it was removed from the analysis. In the PR-BM model, convergence errors were observed for TR5 and TE3. Fig. 8 compares the mean MARE values for temperature and water content predictions, highlighting how the choice of surrogate group and thermodynamic model influences accuracy. Data associated with individual PL surrogates can be found in the SI.

For the temperature predictions, shown in Fig. 8a, most molecular groups performed comparably similar, with the exception of group D-E

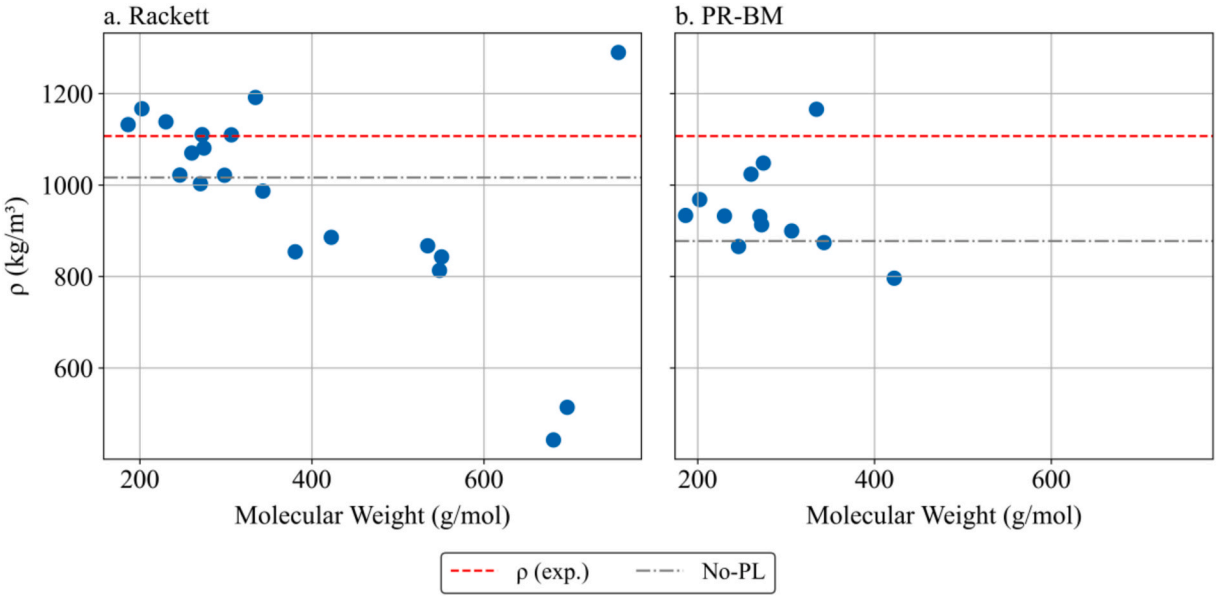

Fig. 7. Liquid density (ρ) predictions of mixture featuring different PL surrogate molecules. (a) Using the Rackett method; (b) using the PR-BM model.

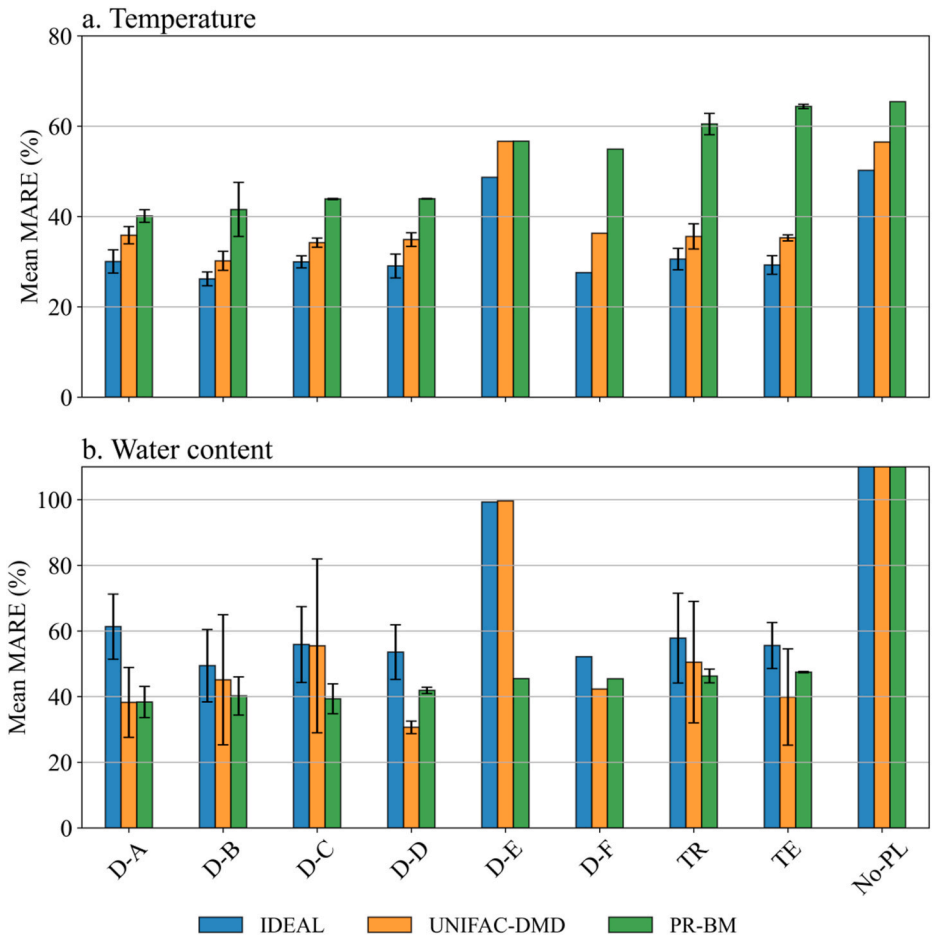

Fig. 8. Mean MARE values for (a) temperature and (b) water content prediction across surrogate groups using IDEAL, UNIFAC-DMD, and PR-BM models. Representative molecular structures are provided in Fig. 3.

that clearly showed the worst performance. Regarding the influence of thermodynamic models, IDEAL consistently achieved the best performance (with MARE values often below 30 %), closely followed by UNIFAC-DMD which showed similar performance in several groups, while PR-BM consistently produced the highest deviations (>40 %). This is surprising given that the IDEAL mixture model neglects intermolecular interactions, which are typically considered critical for representing PL behavior. The comparatively lower deviations may arise from compensating effects in the simplified model formulation, as well as from uncertainties in molecular definitions and interaction parameters affecting more complex models; therefore, its apparent superior performance should be interpreted with care. The absence of a PL surrogate (No-PL) led to significantly higher deviations (>50 %), underscoring the importance of including a representative for this fraction in the mixture. Variability within groups was generally small, with the exception of group D-B for the PR-BM model, suggesting that functional group variations may have little effect on temperature predictions.

Fig. 8b shows the deviations for the evolution of the water content predictions. In contrast to the temperature predictions, here the IDEAL model consistently produced the largest errors (>50 %). PR-BM showed comparatively smaller errors compared to its temperature predictions, and was even able to achieve lower errors for D-E, where the other models deviated by almost 100 %. The UNIFAC-DMD model showed a broader error range (30–60 %) and the widest intragroup variation (D-C), yet it also provided the best-performing individual PL surrogates for all groups except the D-E group. These findings suggest that, in contrast to temperature predictions, functional group variations may be more relevant for water content predictions, as reported by Ille et al. [21]. The No-PL case once again produced the highest errors (>100 %), reinforcing the need to include a representative surrogate for the pyrolytic lignin fraction.

3.4. Best pyrolytic lignin surrogate candidates

The best PL surrogate molecules for each property and model are compared in Table 5. While no single PL surrogate excelled across all evaluations, dimers dominated the rankings overall, with the biphenyl group (D-B) consistently ranking among the top performers for most properties and models. Among the biphenyl groups' molecules, D-B1 stands out as appearing in the top rank for most properties and models, achieving the lowest elemental composition error (RE = 4.50 %) and the best temperature prediction under the IDEAL model (MARE = 24.09 %). D-B2 and D-B3 also showed strong performance, reaching error values of 6.70 % and 25.67 %, respectively, for elemental composition and water content predictions. And, it is worth noting that D-B2 (3,4,4-biphenyltriol) was also selected in previous studies by Ille et al. [21] and Krutof and Hawboldt [28] as a representative compound for modeling the pyrolytic lignin in VLE, further supporting its relevance.

Analyzing the bio-oil bulk properties, the elemental composition is best reproduced by surrogates that match the experimental FPBO carbon and oxygen balance (C ≈ 60 wt% and O ≈ 30–35 wt%), which is expected given that these elements dominate the overall bio-oil composition. The best-performing surrogates are all dimers containing two to four oxygen atoms. Regarding density, the Rackett model provides values much closer to the experimental FPBO density than PR-BM, which largely underestimates density for most surrogates. The best

Table 5
Top five performing surrogates across all categories, ranked by lowest error values. Representative molecular structures are provided in Fig. 3.

	Input bio-oil properties					
	C-H-O (wt. %)		Density – Rackett		Density – PR-BM	
	Surrogate	MARE (%)	Surrogate	RE (%)	Surrogate	RE (%)
1	D-B1	4.50	D-B4	0.25	D-A2	5.27
2	D-B2	6.70	D-D2	0.25	D-A4	5.35
3	D-A1	7.39	D-C1	0.25	D-B2	12.5
4	D-E1	8.01	D-B1	2.26	D-B1	15.7
5	D-D2	8.44	D-A4	2.37	D-A1	15.8
	Temperature profile					
	IDEAL		UNIFAC-DMD		PR-BM	
	Surrogate	MARE (%)	Surrogate	MARE (%)	Surrogate	MARE (%)
1	D-B1	24.09	D-B1	28.01	D-B2	36.37
2	D-B3	26.40	D-B2	29.14	D-B1	36.45
3	D-B2	26.47	D-B3	30.70	D-A4	38.67
4	D-D1	27.17	D-B4	32.86	D-A3	39.55
5	D-A4	27.26	D-C2	33.47	D-A1	40.17
	Water content profile					
	IDEAL		UNIFAC-DMD		PR-BM	
	Surrogate	MARE (%)	Surrogate	MARE (%)	Surrogate	MARE (%)
1	D-B3	35.80	D-B3	25.67	D-A4	32.40
2	TR2	39.03	TR2	27.59	D-B2	33.35
3	D-B1	46.34	D-A1	28.47	D-C2	36.12
4	D-A1	47.53	D-D2	29.30	D-A3	36.80
5	D-D2	47.66	TE3	29.53	D-B1	38.59

agreement with Rackett is obtained for D-B4, D-D2 and D-C1 (RE ≈ 0.25 %), while PR-BM performs best for D-A2 and D-A4 (RE ≈ 5.3 %). Notably, the top performers differ between models, indicating that the description of molecular intermolecular interactions plays a central role in density prediction.

For temperature prediction, dimers again show the most consistent performance across all thermodynamic models, with the D-B (biphenyl) structures emerging as the best candidates. D-B1 and D-B2 in particular provide the lowest temperature MAREs under IDEAL and UNIFAC-DMD, while also outperforming most other surrogates in PR-BM. Notably, under the PR-BM model, the top candidates following D-B1 and D-B2 are exclusively D-A (β-O-4) dimers. Based on these observations, it seems that D-B and D-A (in the case of PR-BM) structures better capture the intermediate-to-heavy volatility window that is most relevant for VLE temperature predictions in FPBO.

In the case of water content prediction, the best-performing surrogate molecules varies between thermodynamic models, with IDEAL and UNIFAC-DMD identifying a similar set of top candidates, namely D-B3 and TR2, followed by D-A1 and D-D2. In contrast, PR-BM favors a different group of structures, with D-A4 and D-B2 yielding the lowest deviations. In addition, analysis of the UNIFAC-DMD top performers functional groups shows that the best surrogates exhibit a balance of hydroxyl (-OH) and ether (-O-) groups in their structure. In comparison, the worst performing molecules, reported in the SI, are dominated by hydroxyl groups (-OH).

In addition to the evaluation of errors, the ability to model distillation profiles must also be considered. Fig. 9 compares the top two surrogates for each model and the No-PL case against the experimental ADC data for temperature and water content profiles. The selected profiles highlight how individual surrogates capture the VLE behavior of the pyrolytic lignin fraction, allowing for direct comparison across different thermodynamic models. For clarity, only the top two molecules from each model are shown in the main figures, while the complete top five rankings are provided in the SI.

Regarding the temperature, all PL surrogates tended to underestimate the experimental curve, resulting in a convex shaped simulation profile, consistent with the behavior reported by Krutof and Hawboldt [28]. For the UNIFAC-DMD model (Fig. 9b), D-B2 closely matched the initial distillation temperature, while D-B1 showed a slight underestimation. The IDEAL model (Fig. 9a) overestimated this point, whereas

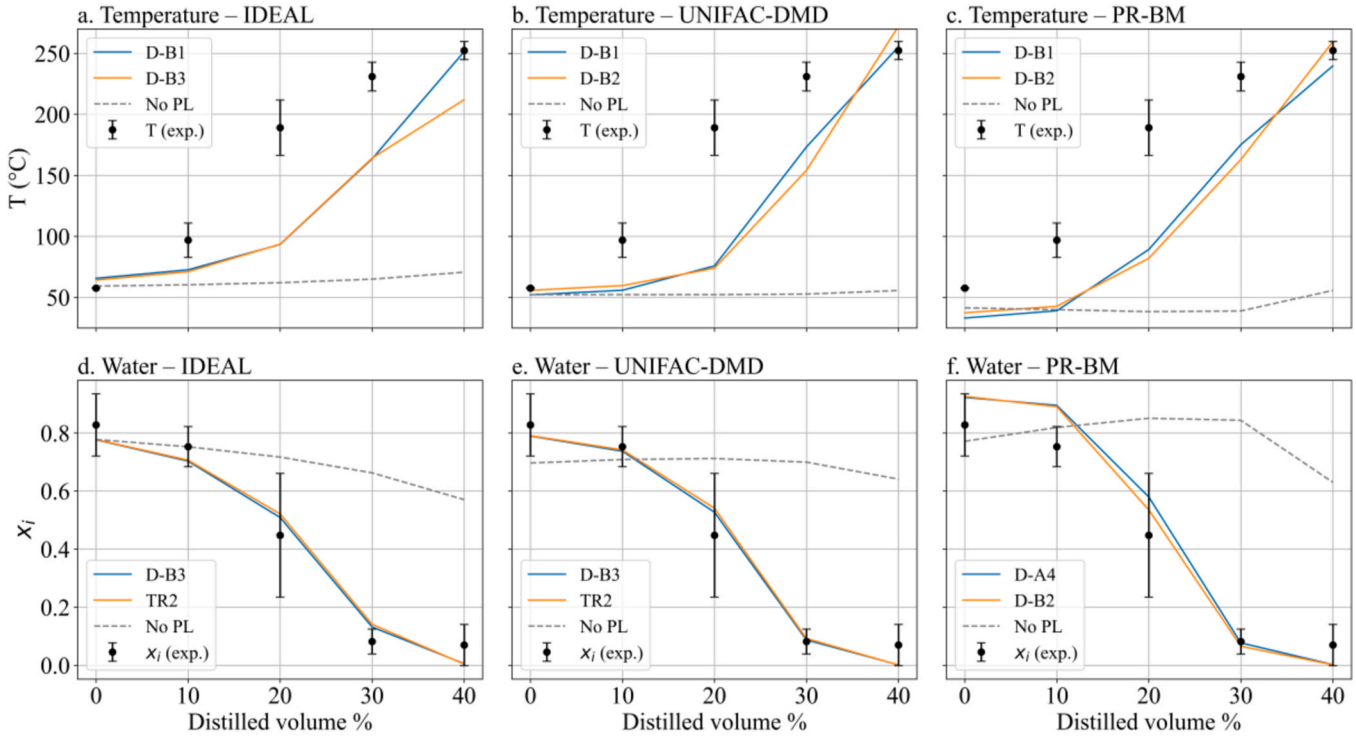

Fig. 9. Simulated ADC temperature and water content profiles for top-performing surrogate molecules and the No-PL case across thermodynamic models: (a) & (d) IDEAL, (b) & (e) UNIFAC-DMD and (c) & (f) PR-BM. Representative molecular structures are provided in Fig. 3.

PR-BM (Fig. 9c) strongly underestimated it. This difference at the initial distillation point contributes to the lower aggregated temperature errors observed for the IDEAL model, whereas the higher errors associated with PR-BM largely result from its strong underestimation of the initial boiling point. All simulated curves fail to capture the sharp temperature rise observed between 10 and 20 vol%. Instead, they consistently underestimate the boiling temperature throughout the distillation and show the steepest incline to the 20-30-40 vol% range, where the experimental curve actually begins to flatten. The last distillation point is well captured by D-B1 in both the IDEAL and UNIFAC-DMD models and by D-B2 in the PR-BM model (Fig. 9a–c).

Compared to the softwood derived FPBO studied by Krutof and Hawboldt [28], the bio-oil investigated here is strongly enriched in lignin derived compounds, which results in lower distillate yields and a substantially steeper experimental temperature profile. As a result, the inability to reproduce this sharp temperature rise is not interpreted as a fundamental limitation of the models, but rather as a consequence of the lignin-rich nature of the bio-oil and the higher contribution of the poorly characterized heavy fraction. Improved agreement would therefore likely require a more detailed representation of the pyrolytic lignin fraction, potentially involving multiple surrogate molecules, together with improved thermodynamic parameters for these surrogates.

While the surrogates still captured key features of the temperature curve, the No-PL case consistently failed to do so, producing a flat and inaccurate profile across all models. This again reaffirms the need to include a pyrolytic lignin surrogate to achieve more accurate VLE predictions.

Fig. 9 d, e, and f show the water content profiles obtained with the different thermodynamic models. All models are able to capture the general trend of the experimental data across the distillation range, with the UNIFAC-DMD model (Fig. 9e) showing the best overall agreement and the lowest errors. Despite its comparatively larger deviations, the IDEAL model (Fig. 9d) follows a curve shape similar to that of UNIFAC-DMD. Higher errors for this model may stem primarily from mismatches at the final distillation points. In contrast, the PR-BM model (Fig. 9f) was the only one to overestimate the water content in the initial stages of the distillation, followed by a sharper decline. Notably, the overall shape of the water content curve remained consistent across different PL surrogates, with the choice of molecule mainly influencing the magnitude of the errors rather than the general trend of the predictions. As with the temperature predictions, the No-PL case failed to capture the experimental trend, producing an inaccurate water content profile across all models.

Evaluating the simulated activity coefficient of water at the first distillation point for molecule D-B1 reveals important differences. For the UNIFAC-DMD model, the predicted γ_{water} was 1.87, which aligns well with the experimentally estimated value of 1.76. This agreement, together with its accurate water content predictions, highlights the model's suitability for capturing non-ideal behavior in fast pyrolysis bio-oils. In contrast, PR-BM predicted a much higher γ_{water} of 6.3 for the same surrogate, correlating with its poor performance in the initial distillation region and suggesting limited applicability for these systems.

It is also important to note that deviations between modeled and experimental curves may also arise from uncertainties in both the experimental procedure and analytical methods. In particular, offsets in temperature and distilled volume readings can contribute to the observed deviations. Additionally, uncertainties in quantification of the fast pyrolysis bio-oil and especially in the small distillate samples can also affect the results.

3.5. Assessment of unknowns

The assessment of the unknown fraction was treated separately from the main VLE error analysis due to its inherently higher uncertainty. The analysis focused on evaluating trends in the predicted profiles, providing qualitative insights rather than quantitative error assessments. Fig. 10 compares the simulated profiles of selected PL surrogates against the experimental distribution of the unknown fraction using the IDEAL, UNIFAC-DMD, and PR-BM models.

Overall, most dimers started to distil around 20 vol%, which aligns well with the experimental profile if we consider that the apparently high concentration of unknowns in the early fractions is likely caused by an underestimation of water content and/or other volatiles. A few dimers, however, showed earlier onset of distillation, particularly D-E1 for all models and D-A1, D-C1 and D-D2 for the IDEAL and UNIFAC-DMD model. Among these, D-E1 exhibited an especially atypical behavior, predicting disproportionately high concentrations of unknowns in the distillate from the very beginning of the distillation. This unusual trend is consistent with D-E1's poorer performance in simulating other properties, suggesting that it may not be a suitable standalone surrogate for representing the PL fraction. For the trimers and tetramers, distillation typically began later, around 30–40 vol%, and in some cases even beyond this range. Among all tested candidates, the surrogate that best captured the overall trend of the unknown fraction was D-A1, followed by D-B3. Additional profiles are provided in the SI.

These findings provide insights into the distillation behavior of the lignin-derived fraction of the bio-oil. While dimers dominate the onset of unknowns release, their contributions are not uniform, with some species exhibiting earlier volatility and others aligning more closely with the mid-distillation range. In contrast, bulkier oligomers contribute

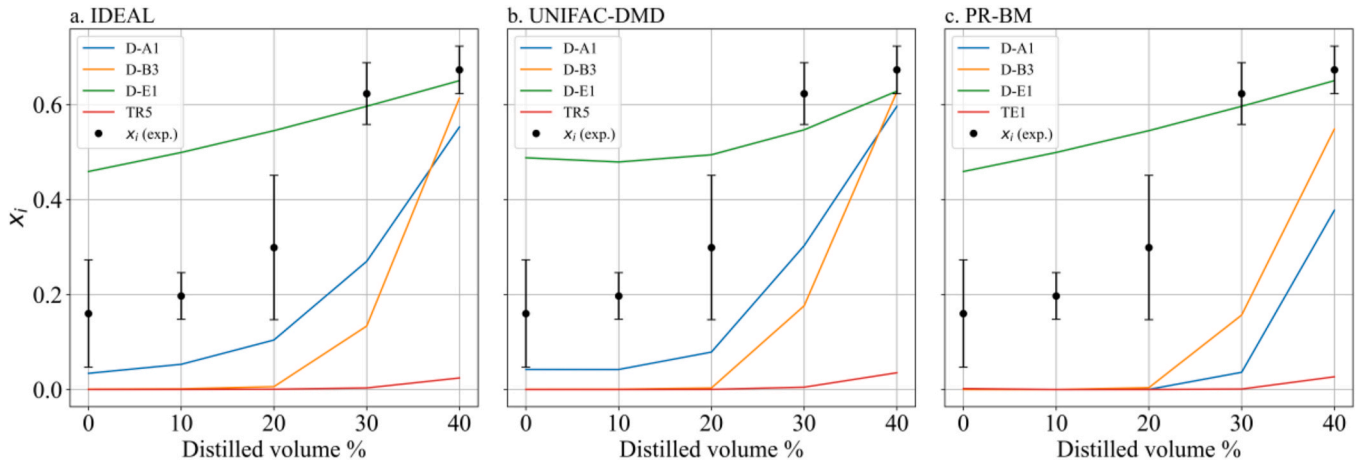

Fig. 10. Simulated ADC unknowns profile for selected PL surrogates across the thermodynamic models (a) IDEAL, (b) UNIFAC-DMD and (c) PR-BM. Representative molecular structures are provided in Fig. 3.

primarily at later stages, reflecting their higher molecular weights. Importantly, even surrogates such as D-E1, despite their unrealistic concentration patterns, could still play a useful role when designing surrogate mixtures with multiple representatives for the PL fractions, as they can contribute to capturing early-distilling behavior. Understanding the distinct contributions of each surrogate enables for a more informed design of surrogate mixtures for the pyrolytic lignin, supporting a more accurate phase equilibrium modeling.

4. Conclusion

In this study, we investigated the phase equilibrium of fast pyrolysis bio-oil (FPBO) by combining advanced distillation curve (ADC) experiments with vapor-liquid equilibrium (VLE) simulations. The influence of various pyrolytic lignin (PL) surrogates was assessed across different thermodynamic models to evaluate their ability to reproduce experimental distillation behavior. These findings contribute to a deeper understanding of FPBO phase behavior and help guide the design of surrogate mixtures that can better predict VLE calculations of FPBO, ultimately improving the predictive accuracy of process simulations.

The results highlight the critical role of surrogate selection in accurately representing the PL fraction. In comparison to the No-PL case, in which no representative for the PL fraction was used, introducing a PL surrogate generally improved model accuracy, particularly for elemental composition and VLE behavior. For the specific case of density predictions, a more cautious selection is recommended, as some surrogates yielded less accurate results than when no surrogate was used.

The evaluation of thermodynamic methods showed that the IDEAL model, despite not accounting for molecular interactions, delivered reasonably good results, including the lowest deviations in the temperature curve. This outcome may be partly attributed to a favorable offset in the initial boiling point, which coincidentally overlaps the experimental data. Overall, its predictions were comparable to those of the UNIFAC-DMD model, which was the most accurate at predicting the water content and also showed consistency with the calculated experimental activity coefficient of water, indicating its suitability for modeling non-ideal behavior in fast pyrolysis bio-oils. In contrast, the PR-BM model consistently showed higher deviations in temperature predictions and frequently delivered inferior performance overall. Furthermore, its strong overestimation of the water activity coefficient suggests that it may be less appropriate for accurately capturing the phase behavior of such systems.

Regarding the molecules, dimers provided the most consistent performance in reproducing FPBO properties and VLE behavior, with the biphenyl-based D-B group ranking among the top performers across most evaluations. Other dimers such as ones from groups D-A (β-O-4) and D-D (phenylcoumaran) also showed strong performance. Trimers and tetramers appeared among the best candidates only for water content prediction under UNIFAC-DMD, where a few molecules (e.g., TR2 and TE3) showed reasonable agreement, but they were less frequently ranked for the remaining properties and occasionally exhibited convergence issues for VLE results, particularly under PR-BM.

The results also revealed a strong dependence between the optimal surrogate choice and the thermodynamic model employed. While IDEAL and UNIFAC-DMD generally favored similar top-performing surrogates, with the D-B group dominating, the PR-BM model showed a preference for group D-A in several cases. Moreover, the optimal surrogate choice also depends on the target property, as different properties emphasize distinct aspects of molecular structure and VLE behavior.

Analysis of the unknown fraction provided further insights into the distillation characteristics of lignin-derived compounds. While some dimers initiate distillation earlier than expected, most remain stable and started distilling around the 20 vol% mark. In contrast, larger oligomers only started distilling at higher distillation volumes (30–40 vol%). Given these differences, mixtures of surrogates with complementary characteristics could help improve how the PL fraction is represented in phase equilibrium simulations in future calculations.

CRediT authorship contribution statement

Ana C.C. Araujo: Writing – original draft, Visualization, Validation, Methodology, Investigation, Data curation, Conceptualization. **Frederico G. Fonseca:** Writing – review & editing, Validation, Methodology. **Nicolaus Dahmen:** Supervision, Funding acquisition. **Axel Funke:** Writing – review & editing, Supervision, Conceptualization.

Acknowledgements

This study was supported by the European Union's Horizon 2020 research and innovation programme under Grant Agreement No. 101007130. The authors would also like to thank Manuel Brislinger for his help in carrying out the ADC experiments, and Birgit Rolli for her assistance with the GC-FID analysis of the ADC samples.

Appendix A. Supplementary data

Supplementary data to this article can be found online at https://doi.org/10.1016/j.biombioe.2026.109009.

Data availability

Data will be made available on request.

References

[1] A.V. Bridgwater, Review of fast pyrolysis of biomass and product upgrading, Biomass Bioenergy 38 (2012) 68–94, https://doi.org/10.1016/j.biombioe.2011.01.048.
[2] T. Bridgwater, Challenges and opportunities in fast pyrolysis of biomass: part I, Johnson Matthey Technol. Rev. 62 (2018) 118–130, https://doi.org/10.1595/205651318X696693.
[3] A. Oasmaa, Y. Solantausta, V. Arpiainen, E. Kuoppala, K. Sipilä, Fast pyrolysis bio-oils from wood and agricultural residues, Energy Fuel. 24 (2010) 1380–1388, https://doi.org/10.1021/ef901107f.
[4] X. Hu, M. Gholizadeh, Progress of the applications of bio-oil, Renew. Sustain. Energy Rev. 134 (2020) 110124, https://doi.org/10.1016/j.rser.2020.110124.
[5] A.P. Pinheiro Pires, J. Arauzo, I. Fonts, M.E. Domine, A. Fernández Arroyo, M. E. Garcia-Perez, J. Montoya, F. Chejne, P. Pfromm, M. Garcia-Perez, Challenges and opportunities for bio-oil refining: a review, Energy Fuel. 33 (2019) 4683–4720, https://doi.org/10.1021/acs.energyfuels.9b00039.
[6] A. Oasmaa, J. Lehto, Y. Solantausta, S. Kallio, Historical review on VTT fast pyrolysis bio-oil production and upgrading, Energy Fuel. 35 (2021) 5683–5695, https://doi.org/10.1021/acs.energyfuels.1c00177.
[7] S. Papari, K. Hawboldt, A review on condensing system for biomass pyrolysis process, Fuel Process. Technol. 180 (2018) 1–13, https://doi.org/10.1016/j.fuproc.2018.08.001.
[8] A.-C. Johansson, K. Iisa, L. Sandström, H. Ben, H. Pilath, S. Deutch, H. Wiinikka, O. G.W. Öhrman, Fractional condensation of pyrolysis vapors produced from Nordic feedstocks in cyclone pyrolysis, J. Anal. Appl. Pyrolysis 123 (2017) 244–254, https://doi.org/10.1016/j.jaap.2016.11.020.
[9] A. Moutsoglou, B. Lawburgh, J. Lawburgh, Fractional condensation and aging of pyrolysis oil from softwood and organosolv lignin, J. Anal. Appl. Pyrolysis 135 (2018) 350–360, https://doi.org/10.1016/j.jaap.2018.08.016.
[10] N.T. Machado, S.A.P.D. Mota, R.A.C. Leão, R.O.M.A.D. Souza, S. Duvoisin Junior, L.E.P. Borges, A.D.A.M.D. Mota, Upgrading/deacidification of bio-oils by liquid–liquid extraction using aqueous methanol as a solvent, Energies 17 (2024) 2713, https://doi.org/10.3390/en17112713.
[11] G.K. Parku, S.R. Pulicanti, A. Funke, N. Dahmen, Phase equilibria aided optimization of levoglucosan extraction during condensation of fast pyrolysis bio-oils, Energy Fuel. 38 (2024) 14343–14350, https://doi.org/10.1021/acs.energyfuels.4c01097.
[12] P. Kostetskyy, L.J. Broadbelt, Progress in modeling of biomass fast pyrolysis: a review, Energy Fuel. 34 (2020) 15195–15216, https://doi.org/10.1021/acs.energyfuels.0c02295.
[13] F.G. Fonseca, A. Funke, Modeling of liquid–vapor phase equilibria of pyrolysis bio-oils: a review, Ind. Eng. Chem. Res. 63 (2024) 13401–13420, https://doi.org/10.1021/acs.iecr.4c00775.
[14] R. Bayerbach, D. Meier, Characterization of the water-insoluble fraction from fast pyrolysis liquids (pyrolytic lignin). Part IV: structure elucidation of oligomeric molecules, J. Anal. Appl. Pyrolysis 85 (2009) 98–107, https://doi.org/10.1016/j.jaap.2008.10.021.

[15] M.B. Figueirêdo, R.H. Venderbosch, H.J. Heeres, P.J. Deuss, In-depth structural characterization of the lignin fraction of a pine-derived pyrolysis oil, J. Anal. Appl. Pyrolysis 149 (2020) 104837, https://doi.org/10.1016/j.jaap.2020.104837.
[16] B. Scholze, D. Meier, Characterization of the water-insoluble fraction from pyrolysis oil (pyrolytic lignin). Part I. PY–GC/MS, FTIR, and functional groups, J. Anal. Appl. Pyrolysis 60 (2001) 41–54, https://doi.org/10.1016/S0165-2370(00)00110-8.
[17] W.R. Silva, T.M. Santos, J.C. Carregosa, C.C. Schmitt, K. Raffelt, N. Dahmen, A. Wisniewski, Bio-oil as a source of renewable chemicals: the chemistry of pyrolytic lignin, Biomass Conv. Bioref. (2024), https://doi.org/10.1007/s13399-024-05622-1.
[18] M.B. Figueirêdo, I. Hita, P.J. Deuss, R.H. Venderbosch, H.J. Heeres, Pyrolytic lignin: a promising biorefinery feedstock for the production of fuels and valuable chemicals, Green Chem. 24 (2022) 4680–4702, https://doi.org/10.1039/D2GC00302C.
[19] A. Oasmaa, T. Sundqvist, E. Kuoppala, M. Garcia-Perez, Y. Solantausta, C. Lindfors, V. Paasikallio, Controlling the phase stability of biomass fast pyrolysis bio-oils, Energy Fuel. 29 (2015) 4373–4381, https://doi.org/10.1021/acs.energyfuels.5b00607.
[20] M. Li, M. Zhang, Y. Yu, H. Wu, Ternary system of pyrolytic lignin, mixed solvent, and water: phase diagram and implications, Energy Fuel. 32 (2018) 465–474, https://doi.org/10.1021/acs.energyfuels.7b02943.
[21] Y. Ille, F. Kröhl, A. Velez, A. Funke, S. Pereda, K. Schaber, N. Dahmen, Activity of water in pyrolysis oil—Experiments and modelling, J. Anal. Appl. Pyrolysis 135 (2018) 260–270, https://doi.org/10.1016/j.jaap.2018.08.027.
[22] M.R. Salas, F.G. Fonseca, A.C.C. De Araujo, M. García-Perez, A. Funke, Liquid–liquid equilibrium prediction in fast pyrolysis bio-oil systems: a framework for incorporating bio-oil complexity, Energy Fuel. 38 (2024) 18769–18780, https://doi.org/10.1021/acs.energyfuels.4c03387.
[23] Y. Yu, Y.W. Chua, H. Wu, Characterization of pyrolytic sugars in bio-oil produced from biomass fast pyrolysis, Energy Fuel. 30 (2016) 4145–4149, https://doi.org/10.1021/acs.energyfuels.6b00464.
[24] Z. Xiong, J. Guo, W. Chaiwat, W. Deng, X. Hu, H. Han, Y. Chen, K. Xu, S. Su, S. Hu, Y. Wang, J. Xiang, Assessing the chemical composition of heavy components in bio-oils from the pyrolysis of cellulose, hemicellulose and lignin at slow and fast heating rates, Fuel Process. Technol. 199 (2020) 106299, https://doi.org/10.1016/j.fuproc.2019.106299.
[25] I. Fonts, M. Atienza-Martínez, H.-H. Carstensen, M. Benés, A.P. Pinheiro Pires, M. Garcia-Perez, R. Bilbao, Thermodynamic and physical property estimation of compounds derived from the fast pyrolysis of lignocellulosic materials, Energy Fuel. 35 (2021) 17114–17137, https://doi.org/10.1021/acs.energyfuels.1c01709.
[26] M. Rojas, F.G. Fonseca, U. Hornung, A. Funke, N. Dahmen, Synthetic lignin oligomers: analytical techniques, challenges, and opportunities, ChemSusChem 18 (2025), https://doi.org/10.1002/cssc.202402334.
[27] E. Terrell, Estimation of fuel properties for the heavy fraction of biomass pyrolysis oil consisting of proposed structures for pyrolytic lignin and humins, Energies 17 (2024) 2011, https://doi.org/10.3390/en17092011.
[28] A. Krutof, K.A. Hawboldt, Thermodynamic model of fast pyrolysis bio-oil advanced distillation curves, Fuel 261 (2020) 116446, https://doi.org/10.1016/j.fuel.2019.116446.
[29] T.J. Bruno, Improvements in the measurement of distillation curves. 1. A composition-explicit approach, Ind. Eng. Chem. Res. 45 (2006) 4371–4380, https://doi.org/10.1021/ie051393j.
[30] B.C. Windom, T.J. Bruno, Improvements in the measurement of distillation curves. 5. Reduced pressure advanced distillation curve method, Ind. Eng. Chem. Res. 50 (2011) 1115–1126, https://doi.org/10.1021/ie101784g.
[31] T.J. Bruno, L.S. Ott, T.M. Lovestead, M.L. Huber, Relating complex fluid composition and thermophysical properties with the advanced distillation curve approach, Chem. Eng. Technol. 33 (2010) 363–376, https://doi.org/10.1002/ceat.200900562.
[32] A.C.C.D. Araujo, A. Funke, A. Margellou, K. Triantafyllidis, N. Dahmen, Pilot scale fast pyrolysis of lignin in a twin-screw reactor, Biomass Bioenergy 200 (2025) 108041, https://doi.org/10.1016/j.biombioe.2025.108041.
[33] E. Henrich, N. Dahmen, F. Weirich, R. Reimert, C. Kornmayer, Fast pyrolysis of lignocellulosics in a twin screw mixer reactor, Fuel Process. Technol. 143 (2016) 151–161, https://doi.org/10.1016/j.fuproc.2015.11.003.
[34] Aspen Technology, Inc., Aspen Plus® V14 – Physical Property Methods and Models, 2024.
[35] C.W. Lahive, P.C.J. Kamer, C.S. Lancefield, P.J. Deuss, An introduction to model compounds of lignin linking motifs; synthesis and selection considerations for reactivity studies, ChemSusChem 13 (2020) 4238–4265, https://doi.org/10.1002/cssc.202000989.
[36] R. Hempfling, H.-R. Schulten, Chemical characterization of the organic matter in forest soils by curie point pyrolysis-GC/MS and pyrolysis-field ionization mass spectrometry, Org. Geochem. 15 (1990) 131–145, https://doi.org/10.1016/0146-6380(90)90078-E.
[37] R. Manrique, E. Terrell, P. Kostetskyy, F. Chejne, M. Olarte, L. Broadbelt, M. García-Pérez, Elucidating biomass-derived pyrolytic lignin structures from demethylation reactions through density functional theory calculations, Energy Fuel. 37 (2023) 5189–5205, https://doi.org/10.1021/acs.energyfuels.2c04292.
[38] E. Ranzi, P.E.A. Debiagi, A. Frassoldati, Mathematical modeling of fast biomass pyrolysis and bio-oil formation. Note I: kinetic mechanism of biomass pyrolysis, ACS Sustainable Chem. Eng. 5 (2017) 2867–2881, https://doi.org/10.1021/acssuschemeng.6b03096.
[39] J. Prothmann, P. Spégel, M. Sandahl, C. Turner, Identification of lignin oligomers in kraft lignin using ultra-high-performance liquid chromatography/high-resolution multiple-stage tandem mass spectrometry (UHPLC/HRMSn), Anal. Bioanal. Chem. 410 (2018) 7803–7814, https://doi.org/10.1007/s00216-018-1400-4.
[40] B. Scholze, C. Hanser, D. Meier, Characterization of the water-insoluble fraction from fast pyrolysis liquids (pyrolytic lignin), J. Anal. Appl. Pyrolysis 58–59 (2001) 387–400, https://doi.org/10.1016/S0165-2370(00)00173-X.
[41] O.C. Bridgeman, E.W. Aldrich, Vapor pressure tables for water, J. Heat Tran. 86 (1964) 279–286, https://doi.org/10.1115/1.3687121.